Rydberg spectroscopy of a Rb MOT in the presence of applied or ion created electric fields

M. Viteau,[1] J. Radogostowicz,[2], M. G. Bason,[1] N. Malossi,[2] D. Ciampini,[2] O. Morsch,[1] and E. Arimondo[1,2,*]

[1] *INO-CNR, Dipartimento di Fisica E. Fermi, Università di Pisa, Largo Pontecorvo 3, I-56127 Pisa, Italy*

2 *CNISM UdR Pisa, Dipartimento di Fisica E. Fermi, Università di Pisa, Largo Pontecorvo 3, I-56127 Pisa, Italy*

**arimondo@df.unipi.it*

Abstract: Rydberg spectroscopy of rubidium cold atoms trapped in a magneto-optical trap (MOT) was performed in a quartz cell. When electric fields acting on the atoms generated by a plate external to the cell were continuously applied, electric charges on the cell walls were created, as monitored on the Rydberg spectra. Avoiding accumulation of the charges and realizing good control over the applied electric field was instead obtained when the fields were applied only for a short time, typically a few microseconds. In a two-photon excitation via the 6^2P state to the Rydberg state, the laser resonant with the 5^2S-6^2P transition photoionizes the excited state. The photoionization-created ions produce an internal electric field which deforms the excitation spectra, as monitored on the Autler-Townes absorption spectra.

OCIS codes: (020.1475) Bose-Einstein condensates; (020.5780) Rydberg states.

References and links

1. T. F. Gallagher, *Rydberg Atoms*, (Cambridge University Press, Cambridge, 1994).
2. D. Jaksch, J. I. Cirac, P. Zoller, S. L. Rolston, R. Côté, and M. D. Lukin, "Fast Quantum Gates for Neutral Atoms," Phys. Rev. Lett. **85**, 2208 (2000).
3. M. D. Lukin, M. Fleischhauer, R. Côté, L. M. Duan, D. Jaksch, J. I. Cirac, and P. Zoller, "Dipole Blockade and Quantum Information Processing in Mesoscopic Atomic Ensembles," Phys. Rev. Lett. **87**, 037901 (2001).
4. M. Saffman, T. G. Walker, and K. Molmer, "Quantum information with Rydberg atoms," Rev. Mod. Phys. **82**, 2313 (2010).
5. T. Pohl, E. Demler, and M. D. Lukin, "Dynamical Crystallization in the Dipole Blockade of Ultracold Atoms," Phys. Rev. Lett. **104**, 043002 (2010).
6. R. Côté, A. Russell, E. E. Eyler, and P. L. Gould, "Quantum random walk with Rydberg atoms in an optical lattice," N. J. Phys. **8**, 156 (2006).
7. H. Weimer, M. Müller, I. Lesanovsky, P. Zoller, and H. P. Büchler, "A Rydberg quantum simulator," Nat. Phys. **101**, 250601 (2010).
8. B. Olmos, R. González-Férez, and I. Lesanovsky, "Fermionic Collective Excitations in a Lattice Gas of Rydberg Atoms," Phys. Rev. Lett. **103**, 185302 (2009).
9. D. Comparat and P. Pillet, "Dipole blockade in a cold Rydberg atomic sample," J. Opt. Soc. Am. B **27**, A208 (2010), and references therein.
10. R. Heidemann, U. Raitzsch, V. Bendkowsky, B. Butscher, R. Löw, and T. Pfau, "Rydberg Excitation of Bose-Einstein Condensates," Phys. Rev. Lett. **100**, 033601 (2008).
11. E. Urban, T. A. Johnson, T. Henage, L. Isenhower, D. D. Yavuz, T. G. Walker and M. Saffman, "Observation of Rydberg blockade between two atoms," Nat. Phys. **5**, 110 (2009).

#137237 - $15.00 USD Received 1 Nov 2010; revised 24 Nov 2010; accepted 2 Dec 2010; published 17 Mar 2011

12. A. Gaëtan, Y. Miroshnychenko, T. Wilk, A. Chotia, M. Viteau, D. Comparat, P. Pillet, A. Browaeys, and P. Grangier, "Observation of collective excitation of two individual atoms in the Rydberg blockade regime," Nat. Phys. **5**, 115 (2009).
13. T. Wilk, A. Gaëtan, C. Evellin, J. Wolters, Y. Miroshnychenko, P. Grangier, and A. Browaeys, "Entanglement of Two Individual Neutral Atoms Using Rydberg Blockade," Phys. Rev. Lett. **104**, 010502 (2010).
14. L. Isenhower, E. Urban, X.L. Zhang, A.T Gill, T. Henage, T. A. Johnson, T. G. Walker, and M. Saffman, "Demonstration of a Neutral Atom Controlled-NOT Quantum Gate," Phys. Rev. Lett. **104**, 010503 (2010).
15. I. Bloch, "Quantum coherence and entanglement with ultracold atoms in optical lattices," Nature **453**, 1016 (2008).
16. H. Lignier, C. Sias, D. Ciampini, Y. Singh, A. Zenesini, O. Morsch, and E. Arimondo, "Dynamical Control of Matter-Wave Tunneling in Periodic Potential," Phys. Rev. Lett. **99**, 220403 (2007).
17. M. Viteau, J. Radogostowicz, A. Chotia, M. Bason, N. Malossi, F. Fuso, D. Ciampini, O. Morsch, I. I. Ryabtsev, and E.Arimondo, "Ion detection in the photoionization of a Rb BoseEinstein condensate," J. Phys. At. Mol. Opt. Phys. **43**, 155301 (2010).
18. B. K. Teo, D. Feldbaum, T. Cubel, J. R. Guest, P. R. Berman, and G. Raithel, "Autler-Townes spectroscopy of the $5S_{1/2} - 5P_{3/2} - 44D$ cascade of cold ^{85}Rb atoms," Phys. Rev. A **68**, 053407 (2003).
19. A. A. Grabowski, A R. Heidemann, A R. Löw, A J. Stuhler, A T. Pfau, "High resolution Rydberg spectroscopy of ultracold rubidium atoms," Fortschr. Phys. **54**, 765–775 (2006).
20. K. Singer, M. Reetz-Lamour, T. Amthor, L. G. Marcassa, and M. Weidemüller, "Suppression of Excitation and Spectral Broadening Induced by Interactions in a Cold Gas of Rydberg Atoms," Phys. Rev. Lett. **93**, 163001 (2004).
21. C. Ates, T. Pohl, T. Pattard, and T. J. M. Rost, "Many-body theory of excitation dynamics in an ultracold Rydberg gas," Phys. Rev. A **76**, 013413 (2007).
22. A. Chotia, M. Viteau, T. Vogt, D. Comparat, and P. Pillet, "Kinetic Monte Carlo modeling of dipole blockade in Rydberg excitation experiment," N. J. Phys. **10**, 045031 (2008).
23. D. B. Branden, T. Juhasz, T. Mahlokozera, C. Vesa, R. O. Wilson, M. Zheng, A. Kortyna, and D. A. Tate, "Radiative lifetime measurements of rubidium Rydberg states," J. Phys. At. Mol. Opt. Phys. **43**. 010502 (2010), and references therein.
24. E. Courtade, M. Anderlini, D. Ciampini, J. H. Müller, O. Morsch, E. Arimondo, M. Aymar, and E. J. Robinson, "Two-photon ionization of cold rubidium atoms with a near resonant intermediate state," J. Phys. At. Mol. Opt. Phys. **37**, 967 (2004).
25. M. Saffman and T. G. Walker, "Analysis of a quantum logic device based on dipole-dipole interactions of optically trapped Rydberg atoms," Phys. Rev. A **72**, 022347 (2005).
26. W. Li, P. L. Tanner, and T. F. Gallagher, "Dipole-Dipole Excitation and Ionization in an Ultracold Gas of Rydberg Atoms," Phys. Rev. Lett. **94**, 173001 (2005).
27. M. S. O'Sullivan and B. P. Stoicheff, "Scalar polarizabilities and avoided crossings of high Rydberg states in Rb," Phys. Rev. A **31**, 2718 (1985).
28. M. S. O'Sullivan and B. P. Stoicheff, "Scalar and tensor polarizabilities of ^2D states in Rb," Phys. Rev. A **33**, 1640 (1986).
29. C. Cohen-Tannoudji, J. Dupont-Roc, and G. Grynberg, *Atom-Photon Interactions* (Wiley-Interscience Publications, NewYork, 1992).
30. T. Amthor, C. G. Christian, C. S. Hofmann, and M. Weidemüller, "Evidence of Antiblockade in an Ultracold Rydberg Gas," Phys. Rev. Lett. **104**, 013001 (2010).
31. W. I. Mourachko, M. W. Noel, and T. F. Gallagher, "Millimeter-wave spectroscopy of cold Rb Rydberg atoms in a magneto-optical trap: Quantum defects of the ns, np, and nd series," Phys. Rev. A **67**, 052502 (2003).
32. A. K. Mohapatra, T. R. Jackson, and C. S. Adams, "Coherent Optical Detection of Highly Excited Rydberg States Using Electromagnetically Induced Transparency," Phys. Rev. Lett. **98**, 113003 (2007).
33. M. A. Bouchiat, J. Guéna, Ph. Jacquier, M. Lintz, and A. V. Papoyan, "Electrical conductivity of glass and sapphire cells exposed to dry cesium vapor," Appl. Phys. B **68**, 1109 (1999).
34. L. Oster, V. Yaskolko, and J. Haddad, "Classification of Exoelectron Emission Mechanisms," Phys. Stat. Solidi A **174**, 431 (1999).

1. Introduction

In recent years, Rydberg atoms have been the subject of intense study [1] and have become an important tool for several branches of quantum physics such as quantum-information processing with neutral atoms [2–4], production of single-atom as well as single-photon sources [3, 5], implementation of quantum random walks in an optical lattice [6], quantum simulation of complex spin systems [7] and the creation of entangled many-particle states [8]. All these proposals are based on the dipole blockade mechanism where the strong Rydberg dipole-dipole interac-

#137237 - $15.00 USD Received 1 Nov 2010; revised 24 Nov 2010; accepted 2 Dec 2010; published 17 Mar 2011

tions control or block a second Rydberg excitation following a first one. The Rydberg excitation blockade was realized in clouds of cold atoms [9] as well as in a Bose Einstein condensate [10]. In addition the excitation of two individual atoms in the Rydberg blockade regime was recently performed [11, 12] and their entanglement demonstrated [13, 14].

The scalability of a quantum computer based on the long-range interactions of Rydberg atoms will rely on the realization of an array of trapped atoms [4]. An optical lattice loaded with one atom in each site, such as the Mott insulator phase of ultracold bosonic atoms, represents the realization such an array. Additional crucial issues to be solved in order to realize this quantum computation configuration are the initialization and readout operations on a single site of the lattice. The preparation of a Mott insulator relies on an apparatus having a large optical access [15]. Such optical access is also required in order to achieve the high quality control of atomic excitations required for the quantum computation operations.

This work reports on Rydberg spectroscopy performed on cold ^{87}Rb atoms in a MOT. The experiments are performed within a Bose-Einstein condensation apparatus based on a quartz cell, used for in previous optical lattice investigations [16]. Because the dipole blockade mechanism is modified by weak electric fields [9] we present an investigation of the atomic response to external electric fields at the mV/cm level. We present an original approaches applied in order to reach a level of control of Rydberg excitation for ultracold atoms as similar to that reached in Ref. [19]. Our control will be of some use for subsequent work on the Rydberg excitation of a Bose-Enstein condensate loaded into an optical lattice.

Our Rydberg detection scheme is based on the ionization of Rydberg states by an electric field. In fact our apparatus allowed measurements of ions generated from MOT and BEC photoionization, with a large detection efficiency [17]. In contrast to Ref. [19] in the present investigation the plates used to apply the ionizing electric field are located outside the quartz cell. Screening of this electric field was directly measured on the Rydberg excitation spectra. This effect is due to the presence of charges on the cell walls, however the source of such charges is not well defined. We demonstrate that even if the voltage applied to the outside of the cell is partially shielded by the charges on the quartz walls, a high level of control is achieved for the electric field acting on the atoms. Care must be taken not to charge the cell due to the prolonged exposure to high voltages. The lifetime of the wall charges is around ten minutes, therefore the electric field was switched for a time shorter than the charge relaxation time.

In order to measure precisely the atomic Rabi frequencies associated with the applied laser light, we measured the Autler-Townes splitting of the Rydberg excitation spectra as in Refs. [18, 19]. The reported spectra are modified by the electric field generated by the ions produced by the laser excitation, as pointed out in Refs. [20–22]. A precise control of the ion production is required for a controlled dipole blockade.

Section 2 introduces the relevant atomic energy levels and the two-photon laser interaction producing the Rydberg excitation. Section 3 describes the experimental configuration for cold atom production, their Rydberg state preparation and their detection by ion collection. Section 4 presents examples of observed Rydberg spectra. The spectra modification produced by the applied electric fields demonstrates the presence of charges on the cell walls following a continuous application of voltage on the external plates. This disturbance is avoided by applying short duration voltage pulses. The measurement of the Rydberg state Stark maps allowed us to calibrate the applied electric field. Autler-Townes spectra are measured and their deformation by the ion generated electric field is analyzed through a simple model. Section 5 presents our conclusions.

#137237 - $15.00 USD Received 1 Nov 2010; revised 24 Nov 2010; accepted 2 Dec 2010; published 17 Mar 2011

2. Atom-laser interactions

^{87}Rb atoms in the $5S_{1/2}$ $(F=2)$ ground level, denoted as $|g\rangle$ with zero energy, are excited to Rydberg state by means of 2-photon absorption, as shown in Fig. 1. The $6^2P_{3/2}$ $(F=3)$ intermediate state, denoted as $|e\rangle$ with energy E_e and decay rate $\Gamma_e = 8.9\times10^6$ s^{-1}, is excited by 421 nm blue radiation. This 421 excitation is characterized by frequency $\nu_{bl} \approx E_e/h$, detuning $\delta_{bl} = \nu_{bl} - E_e/h$, Rabi frequency Ω_{bl}, all of them to be measured in MHz. A second infrared (IR) laser at 1004-1020 nm is required to reach Rydberg states n^2S $(J=1/2)$ and n^2D $(J=3/2,5/2)$, denoted as $|nL\rangle$, with principal quantum number $n=30-80$, having an energy E_{nL} and decay rate Γ_{nL}. The parameters associated with this IR excitation are the frequency $\nu_{IR} \approx (E_{nL}-E_e)/h$, detuning $\delta_{IR} = \nu_{IR} - (E_{nL}-E_e)/h$, Rabi frequency Ω_{IR}. The one photon transitions occur at $\delta_{bl} \approx 0$ and $\delta_{IR} \approx 0$, respectively. The sequence of the two processes produces the $|g\rangle \rightarrow |e\rangle \rightarrow |nL\rangle$ two-step excitation. The two-photon direct excitation $|g\rangle \rightarrow |nL\rangle$ takes place for $\nu_{bl}+\nu_{IR} \approx E_{nL}/h$, or alternatively $\delta_{bl}+\delta_{IR} \approx 0$.

Table 1. Parameters of the explored Rydberg states

Transition $6^2P_{3/2} \rightarrow nL$	Γ_0 (s^{-1})	Γ_{BBR} (s^{-1})	$A(nL \rightarrow 6^2P_{3/2})$ (s^{-1})	Dipole Moment (e a_0 units)
$52S_{1/2}$	6.07×10^3	7.85×10^3	1.2×10^3	2.47×10^{-2}
$53D_{3/2}$	7.02×10^3	5.60×10^3	4.78×10^2	3.51×10^{-2}
$53D_{5/2}$	7.07×10^3	5.40×10^3	4.73×10^2	3.49×10^{-2}

The Γ_{nL} effective decay rate of the nL Rydberg level is given by the sum of the Γ_0, the total spontaneous emission rate, and Γ_{BBR}, the depopulation rate induced by black body radiation (BBR) [23]

$$\Gamma_{nL} = \Gamma_0 + \Gamma_{BBR}. \tag{1}$$

Γ_0 is determined by the $A(nL \rightarrow n'L')$ Einstein coefficients from the $|nL>$ level to all lower-lying levels

$$\Gamma_0 = \sum_{n'L' \neq nL} A(nL \rightarrow n'L'). \tag{2}$$

Γ_{BBR} at the temperature T is written in a similar form, including both lower and higher states

$$\Gamma_{BBR} = \sum_{n'L' \neq nL} A(nL \rightarrow n'L') \frac{1}{exp\left(\frac{E_{nL}-E_{n'L'}}{kT}\right)-1} \tag{3}$$

The $A(nL \rightarrow 6^2P_{3/2})$ spontaneous decay rate from the Rydberg level to all the Zeeman states of the $6^2P_{3/2}$ level determines the transition dipole moment, appearing in the definition of the Ω_{IR} and I_{IR}^{sat} quantities. The atomic parameters for the few Rydberg states investigated are listed in Table 1.

The Rabi frequencies of the $|g\rangle \rightarrow |e\rangle \rightarrow |nL\rangle$ transitions depend on the quantum numbers of the atomic states composing the excitation sequence. For the $|g\rangle = 5^2S_{1/2}(F=2)$ and $|e> = 6^2P_{3/2}(F'=3)$ states the quantum numbers are the hyperfine ones $|F,m_F\rangle$. Instead for the Rydberg states where the hyperfine splitting is small, the states are characterized by the J,m_J quantum numbers. As a consequence the blue and IR Rabi frequencies should be calculated in two different bases, $|I,J,F,m_F\rangle$ to be denoted by the F,m_F subscript and $|I,m_I,J,m_J\rangle$ to be

#137237 - $15.00 USD Received 1 Nov 2010; revised 24 Nov 2010; accepted 2 Dec 2010; published 17 Mar 2011

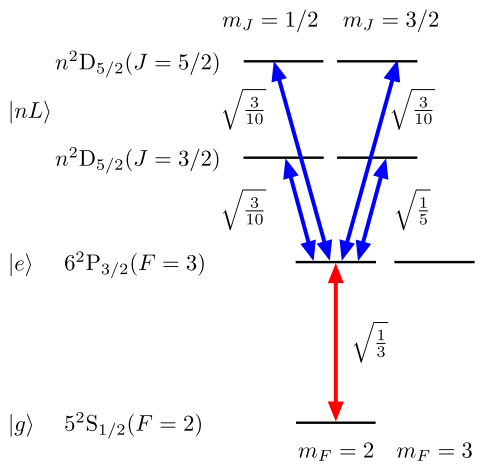

Fig. 1. Atomic states, selection rules imposed by the laser polarization and Clebsch-Gordan coefficients for $5^2\mathrm{S}_{1/2}(F = 2) \rightarrow 5^2\mathrm{P}_{3/2}(F = 3)\rangle \rightarrow n^2\mathrm{D}_{5/2,3/2}$ two-photon excitation, by supposing the blue and IR lasers linearly polarized along the same direction in space parallel to the local magnetic field. The $|F, m_F >$ label shown in the bottom is applied to denote the ^{2}S and ^{2}P states; the $|J, m_J >$ label shown in the top applies to the ^{2}D states. For describing the IR upper excitation the intermediate $n^2\mathrm{P}_{3/2}$ level is decomposed on the $|J, m_J\rangle$ basis as in Eq. (4).

denoted by the I, J subscript. For instance in order to derive the atomic coupling with the IR laser as in Fig. 1, the intermediate $6^2\mathrm{P}_{3/2}(F = 3, m_F = 2)$ state excited by the blue laser should be decomposed into the following states of the $|I, m_I, J, m_J\rangle$ basis:

$$|\frac{3}{2},\frac{3}{2};F=3,m_F=2\rangle_{F,m_F} = \frac{1}{\sqrt{2}}\left(|\frac{3}{2},\frac{3}{2};\frac{3}{2},\frac{1}{2}\rangle_{I,J} + |\frac{3}{2},\frac{1}{2};\frac{3}{2},\frac{3}{2}\rangle_{I,J}\right). \tag{4}$$

As an example, we report in Fig. 1 the laser excitation for the $|g\rangle \rightarrow |e\rangle \rightarrow |n^2D_{5/2,3/2}\rangle$ transitions in the case of blue and IR laser fields with linear polarization along the local magnetic field. The following excitation paths are reported for the $5^2\mathrm{S}_{1/2} \rightarrow 5^2\mathrm{P}_{3/2} \rightarrow n^2\mathrm{D}$ two-photon excitation:

$$5^2S|\frac{1}{2},\frac{3}{2};2,2>_{F,m_F} \rightarrow 6^2P|\frac{3}{2},\frac{3}{2};3,3>_{F,m_F} \rightarrow n^2D|\frac{3}{2},\frac{3}{2};\frac{5}{2};\frac{1}{2}\rangle_{J,m_J}, \tag{5}$$

$$5^2S|\frac{1}{2},\frac{3}{2};2,2>_{F,m_F} \rightarrow 6^2P|\frac{3}{2},\frac{3}{2};3,3>_{F,m_F} \rightarrow n^2D|\frac{3}{2},\frac{1}{2};\frac{5}{2},\frac{3}{2}\rangle_{J,m_J}. \tag{6}$$

The Clebsch-Gordan coefficients associated with the more probable excitation paths are marked in the figure. The dipole moments determining the Ω_{bl} and Ω_{IR} Rabi frequencies are obtained by multiplying the atomic dipole moment by the Clebsch-Gordan coefficient. Laser polarizations orthogonal to the local magnetic field excite a larger number of Zeeman levels. In a MOT all Zeeman levels are populated and owing to the inhomogeneous magnetic field the orientation of the laser field with respect to the local magnetic field is not uniform. A general expression to perform such averages of the Rabi frequencies over the Zeeman levels and the laser polarizations was reported in Ref. [18].

The absorption of a 421 nm photon by an atom in the $6^2\mathrm{P}_{3/2}$ state ionizes the rubidium atoms with an ionization cross-section of 4.7 Mbarn [24], while the cross-section for absorption of 1 μm photon from the $n \approx 50$ Rydberg states is very small, 4.5×10^{-5} Mbarn for 50^2S

#137237 - $15.00 USD Received 1 Nov 2010; revised 24 Nov 2010; accepted 2 Dec 2010; published 17 Mar 2011

and 1.2×10^{-2} Mbarn for 50^2D [25]. We calculated the average number of ions produced by the two-step photoionization pulse from the solution of the master equations describing the atomic interaction with the laser pulses introduced in [24]. As an example the $6^2P_{3/2}$ ionization probability for a 10 μs blue laser pulse is $1.\times10^{-3}$ s^{-1} for a $I_{\rm bl}=30$ W/cm^2 blue laser intensity. In addition, for long duration laser pulses the Penning ionization caused by the interaction-induced motion in cold Rydberg gases is an additional ion source [26].

The atomic absorption spectrum is modified by the presence of electric fields either applied by external sources or internally generated. The electric field polarizabilities of Rb atoms in Rydberg states were measured by Sullivan and Stoicheff in refs. [27,28] respectively for the ^{2}S and ^{2}D states. For instance the scalar polarizability of the 55^2S state is 50(6), for $55^2D_{5/2}$ the scalar and tensorial polarizabilities are respectively 139(8) and 254(10), and for $55^2D_{3/2}$ 85(3) and 82(3) respectively, all polarizabilities are in MHz/(Vcm^{-1})^2 units. The ions generated by laser photoionization of rubidium atoms create an electric field which modifies the absorption of the atoms remaining in the MOT. The MOT ion content is very small, a maximum of one ion per thousand atoms. However at a distance of 1 μm the electric field due to an ion is 0.15 Vcm^{-1}, which represents a -4.4 MHz shift for an atom in state $55^2D_{5/2}, m_J=5/2$, a large value compared to the $\approx$1.5 MHz natural broadening of the $6^2P_{3/2}\rightarrow 55^2D_{5/2}$ transition. The ion electric field is inhomogeneous over the atomic cloud, and we calculated an average value of the electric field acting on the rubidium atoms by supposing that the ions are uniformly distributed within the cold atom cloud. Because the ion number created by the photoionization increases within the laser pulse length, we based our analysis on the pulse mean number. The ions created by the laser irradiation may escape from the atomic cloud under the action of the internal electric fields produced by the electrons and ions, and the escape time should be compared to the Rydberg excitation time.

In a three-level system the saturation of one transition by a strong laser field, i.e. a large Rabi frequency, produces a strong modification of the absorption spectrum on the second transition. Consequence of this strong coupling is the well known Autler-Townes splitting [29]. We investigate the Autler-Townes splitting produced by a strong blue laser and monitor it on the IR transition. If the blue laser is resonant with the $|g>\rightarrow|e>$ transition, the IR transition is splitted into two components separated by the blue laser Rabi frequency, $\Omega_{\rm bl}$, corresponding to the Autler-Townes splitting. For a blue laser beam detuned from the $|g>\rightarrow|e>$ resonance by $\delta_{\rm bl}$, the Autler-Townes modification of the spectrum leads to absorption at the following values of the IR detuning

$$\delta_{\rm IR}^{\pm}=-\left(\delta_{\rm bl}\pm\sqrt{\delta_{\rm bl}^2+\Omega_{\rm bl}^2}\right)/2, \tag{7}$$

representing the two-photon and two-step peaks, or viceversa, depending on the $\delta_{\rm bl}$ sign. The H peak heights for the two-photon and two-step processes are given by

$$H_{\rm 2ph} = C\sin^2(\theta/2), \tag{8}$$

$$H_{\rm 2st} = C\cos^2(\theta/2), \tag{9}$$

respectively, with $\tan\theta=\Omega_{\rm bl}/\delta_{\rm bl}$ and C a constant. Notice that the position for the central point of the Autler-Townes peaks given by $\delta_{\rm IR}^{\rm c}=\left(\delta_{\rm IR}^{+}+\delta_{\rm IR}^{-}\right)/2=-\delta_{\rm bl}/2$ is independent of $\Omega_{\rm bl}$. The excitation to the Rydberg states of cold atoms is strongly modified by dipole blockade, where dipolar interactions between atoms in Rydberg states produce a shift of the energy levels and therefore blocks all atomic excitations to the Rydberg state within a volume defined by the blockade radius [9]. Owing to the dipole blockade, in our experimental investigation the efficiency of excitation to the Rydberg state is depressed and is lower than that predicted from the laser excitation of a single atom. The dipole blockade process is modified into an antiblockade

#137237 - $15.00 USD Received 1 Nov 2010; revised 24 Nov 2010; accepted 2 Dec 2010; published 17 Mar 2011

by the Autler-Townes splitting produced by the blue laser, because one component of that splitting, as reported by [30], is shifted towards the resonance for the excitation of a second atom to the Rydberg state.

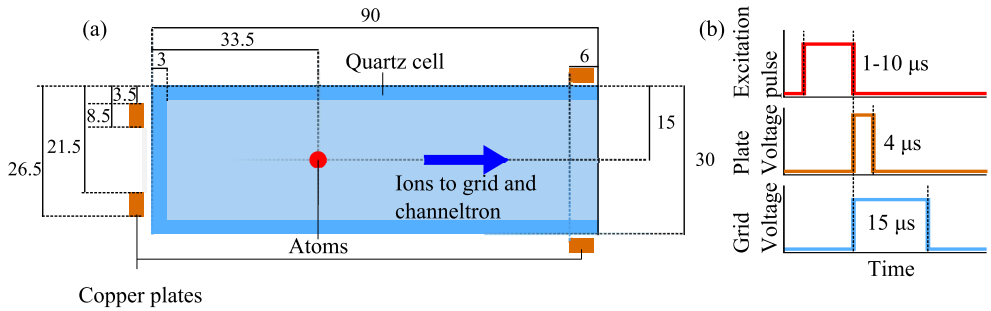

Fig. 2. In (a) schematic of the vacuum quartz and collection system for the ion produced by the MOT/BEC ionization, with dimensions in mm. Notice the copper plates on the front and on the sides of the cell. The grid and the channeltron collecting the ions are located respectively 10 cm and 15 cm from the atomic cloud. The laser beams are combined in order to excite rubidium atoms within the same volume inside the cell. In (b) temporal sequence for the laser excitation, and the application of voltages to the plates and to the accelerating grid is shown.

3. Apparatus

The MOT/BEC apparatus uses two quartz cells, collection and science respectively, horizontally mounted on a central metallic structure [16, 17]. We operate with a MOT having a small size around 50 μm and containing 10^5 atoms at the $\approx 1.5 \times 10^{12}$ cm^{-3} atomic density, in order to investigate conditions similar to those created in a Bose-Einstein condensate.

The 421 nm blue radiation is generated by doubling a MOPA laser (TOPTICA TA 100, with output power 700 mW) with a TOPTICA cavity (output power 60 mW). An infrared (IR) laser between 1000 and 1030 nm allows ionization or atomic excitation to states with quantum number n between 30 and the continuum. High power and frequency stability of the IR radiation is achieved by injection locking a diode on an external cavity (output power 40 mW) into a Sacher TIGER laser (output power 250 mW) where the grating is replaced by a mirror. Both lasers systems, having a line-width smaller that 1 MHz, were locked using a Fabry Perot interferometer where a 780 nm laser locked to the Rb resonance acts as a reference [17]. Both blue and IR beams were focused to a waist larger than the atomic cloud size, the minimum being 100 μm in order to maintain the cloud within the beam waist in presence of fluctuations in the spatial position of the cold atomic cloud. The blue/IR laser beams were applied as a pulse having a 0.5-10 μs duration with a gaussian rise time of 0.08 μs controlled by an acousto-optic modulator.

The MOT magnetic quadrupole field (72 G/cm along the strong axis) was not switched off during the Rydberg excitation phase. Owing to the small MOT size the magnetic field contributed less than 0.2 MHz to the observed linewidths. The polarizations of both blue and IR lasers were linear and parallel to each other along the strong axis of the quadrupole.

The Rydberg atoms are ionized and then detected by applying, just after the Rydberg excitation pulse, an electric field to the cell plates shown in Fig. 2. Experimental results shown in the following SubSection 4.2 provide evidence for the formation of electric charges on the cell walls creating uncontrolled electric fields. In order to avoid the presence of these wall charge,

#137237 - $15.00 USD Received 1 Nov 2010; revised 24 Nov 2010; accepted 2 Dec 2010; published 17 Mar 2011

the Rydberg field ionization was based on an electric field pulse with a rise time of 700 ns and few μs duration applied to the copper plates outside the cell. The ion collection scheme is shown in Fig. 2. In previous work [17] we measured a high collection efficiency $T_h = 0.35(10)$ which includes both the fraction of the produced charges transported to the channel electron multiplier (CEM) and the multiplier detection efficiency. To avoid saturation of the detection system, for the ion spectra reported here a low collection efficiency $T_l = 0.03(1)$ was obtained with the electric field pulse applied only to the plates located far from the CEM.

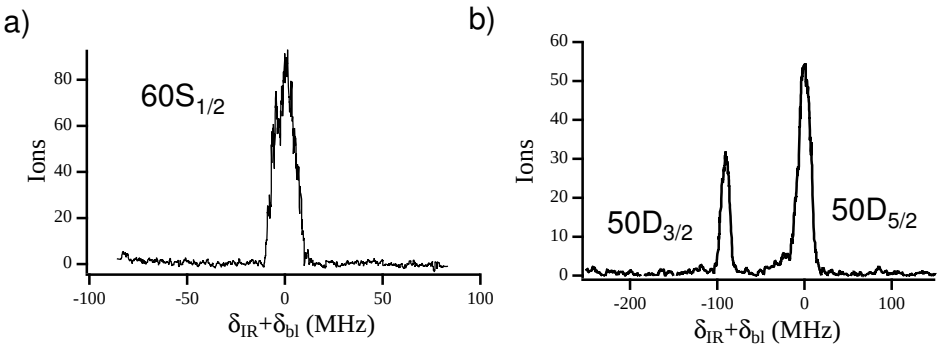

Fig. 3. Detected ion number versus $\delta_{\rm IR}$, the IR laser detuning, produced by the excitation to $60^2S_{1/2}$ level in (a) and to the $50^2D_{3/2,5/2}$ levels in (b). The absolute ion number is determined with a fifteen percent accuracy. The ion spectrum was acquired using 0.5 μs laser pulses and Bbox-car integration of the CEM output signal, Parameters $\delta_{\rm blue} = 200.0$ MHz, $\Omega_{\rm blue} = 7.5$ MHz and $\Omega_{\rm IR} = 0.1$ MHz. The zero value of the $\delta_{\rm IR} + \delta_{bl}$ detuning corresponds to the two-photon excitation from the $5^26_{1/2}(F' = 3)$ level to the $60^2S_{1/2}$ or $50^2D_{5/2}$ Rydberg state.

4. Results

4.1. Rydberg spectra

We investigated the range of Rydberg energy levels we could tune the IR laser to. For this purpose, following excitation to the Rydberg state for the MOT trapped atoms, we measured the ions produced by the field ionization, with small contributions from photoionization, blackbody radiation absorption and Rydberg Penning ionization. Typically we acquired Rydberg spectra by scanning the frequency of the IR laser at fixed frequency of the blue laser. Figures 3 and 4 reports the spectra observed on the produced ions as a function of the IR laser frequency scanned around the the resonant frequency for the Rydberg excitation from the $6^2P_{3/2}(F = 3)$ state. Figure 3 shows the spectrum recorded on the collected ions following the $60^2S_{1/2}$ and $50^2D_{3/2,5/2}$ excitations, respectively.

For the ion signal spectra of Fig. 4 corresponding to the $81^2D_{3/2,5/2}$ excitation, the top spectrum was obtained with no voltage applied to the cell external plates. Because the blue laser was detuned by 60 MHz from the $5^2S_{1/2}(F = 2) \rightarrow 6^2P_{3/2}(F' = 3)$ transition, two-photon and two-step signals are present on the spectrum. The two-photon $5^2S_{1/2}(F = 2) \rightarrow 81^2D_{5/2}$ transition is observed at $\delta_{\rm IR} = -\delta_{\rm bl} = -60$ MHz. The $5^2S_{1/2} \rightarrow 81^2D_{3/2}$ two-photon transition is shifted to a lower frequency by the 81^2D fine splitting. The fine splitting between the $50D_{3/2,5/2}$ and $81^2D_{3/2,5/2}$ levels is in agreement with the predictions of Li *et al.* [31]. The two-step sig-

#137237 - $15.00 USD Received 1 Nov 2010; revised 24 Nov 2010; accepted 2 Dec 2010; published 17 Mar 2011

nal associated to the $6^2P_{3/2}(F'=3) \rightarrow 81^2D_{5/2}$ transition is observed at $\delta_{IR} = 0$ MHz. That associated for the $6^2P_{3/2}(F'=3) \rightarrow 81^2D_{3/2}$ transition is too weak for its observation.

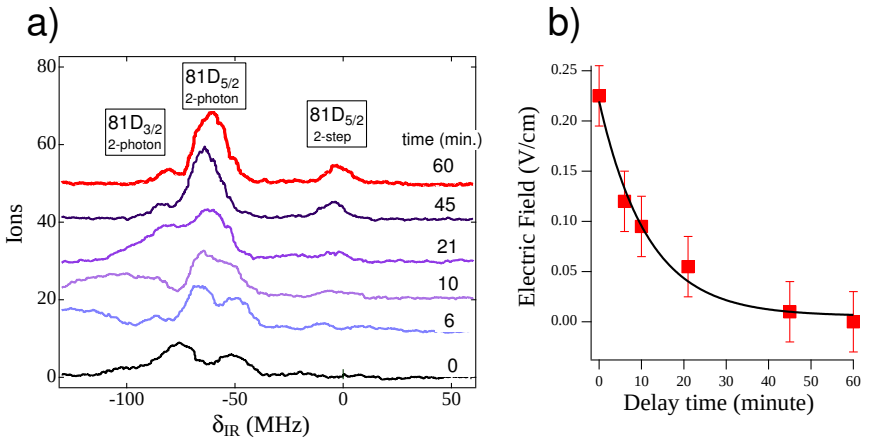

Fig. 4. (a) Detected ion number versus the δ_{IR} IR laser detuning produced by the excitation to the $81^2D_{3/2,5/2}$ Rydberg states. The absolute ion number is determined with a fifteen percent accuracy. Parameters $\delta_{blue} = 60$ MHz, $\Omega_{blue} = 7.5$ MHz and $\Omega_{IR} = 0.1$ MHz. Each spectrum was obtained at the delay time, marked on the right, after the application for 5 seconds 3 kV voltage to the front and lateral plates. The top spectrum was obtained when the space charges on the cell walls disappeared. Other spectra discussed in the text. From left to right $81^2D_{3/2}$ two-photon peak, $81^2D_{5/2}$ two-photon peak and $81^2D_{5/2}$ two-step peak. The two-step $81^2D_{3/2}$ peak is not large enough to be clearly detected. (b) Data (squares) of the electric field acting on the atoms versus delay time, as derived from a Stark map fit to the data in a). Continuous line fit to an exponential decay with time constant 12 ± 1.8 minutes.

4.2. Electric field generated by wall charges

We noticed that the voltage applied to the plates external to the quartz cell created charges on the cell walls that deformed the spectroscopic investigations. A clear example of the role played by the electric field due to the wall charges is shown in Fig. 4a. Rydberg spectra were recorded at different delay times following the application of a 3 kV voltage to the front and lateral plates for five seconds. The bottom spectrum, denoted by 0 time was recorded just after switching off the high voltage. Other spectra were recorded at later times, marked on the right side. A spectrum with clearly identified peaks (top one) was obtained only after 60 minutes, when the charges on the cell walls disappeared. From the analysis of the electric field splitting of the transition we derived that the initial electric field was around 0.2 V/cm and the lifetime of the wall charges was 12 minutes, as shown in Fig. 4b. In order to avoid the influence of these charges and maintain a good detection efficiency associated with the ion guide by the external plate voltage, we rapidly switched on the ion collecting voltages and only during the collection time, with typical pulses in the microsecond range. Formation of wall charges with a screening of an external electric field was reported in Ref. [32], where the main source of charge appeared to be ions and electrons produced by laser photodesorption at the cell surface. Electrical conductivity of the walls for different cells exposed to cesium vapour was investigated in [33], with the conductivity in glass cells connected to the cesium atoms physically adsorbed on the

#137237 - $15.00 USD Received 1 Nov 2010; revised 24 Nov 2010; accepted 2 Dec 2010; published 17 Mar 2011

surface, this process being eliminated using sapphire cells. Notice that in our investigation the charges are produced on a fast time scale determined by the plate voltage risetime, and disappear on the ten minute timescale. We may suppose that the whole process is determined by field-assisted electron emission process, classified as exo-electron emission [34], and charge release from traps associated to rubidium atoms physically adsorbed on the walls. However the relative role of these processes on the time evolution of the wall charges remain obscure.

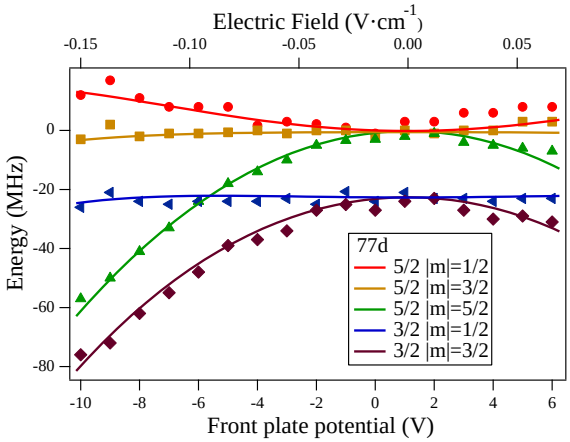

Fig. 5. Stark shift, in MHz, of the Rydberg $77^2D_{3/2,5/2}$ two-photon transitions as function of the externally applied electric field. The zero shift corresponds to the position of the unperturbed $77^2D_{5/2}$ state. Data for the different m_J levels are reported. Notice the presence of avoided crossings between the level energies. The theoretical fit of the shift using the 77^2D electric field polarizability data allowed us the calibration the electric field to the values reported in the top scale.

4.3. Externally applied electric fields

Avoiding an accumulation of charge on the walls we verified the degree of control over the electric field applied to the Rydberg atoms. Rydberg states are very sensitive to the presence of electric fields that produce either a broadening or a splitting of the excitation lines and therefore, at given laser parameters, a modification of the excitation efficiency. We have applied to the external plates low voltages, 10 Volts maximum, and monitored the frequency shift of Rydberg spectra. This constant electric field is applied just during the Rydberg excitation. Results for the measured Stark shift on the $77^2D_{3/2,5/2}$ excitation are shown in Fig. 5. The Stark map reports the measured position of the m_J levels for both D states versus the applied voltage. Notice that the m_J label is correct at zero electric field, while at larger values the electric field mixes the $J = 3/2$ and $J = 5/2$. Notice for an applied electric field around -0.09 Vcm^{-1} the presence of an avoided crossing of the states split by the electric field, similar to those investigated by Sullivan and Stoicheff [28]. The continuous lines based on the polarizabilities by Ref. [28] allowed us to derive the conversion between the applied voltage (bottom axis) and the electric field acting on the atoms (top axis) denoting a minor electric field screening by wall charges. These Stark shifts provide evidence to show that our resolution for the applied electric field is at the 5 mV/cm level.

#137237 - $15.00 USD Received 1 Nov 2010; revised 24 Nov 2010; accepted 2 Dec 2010; published 17 Mar 2011

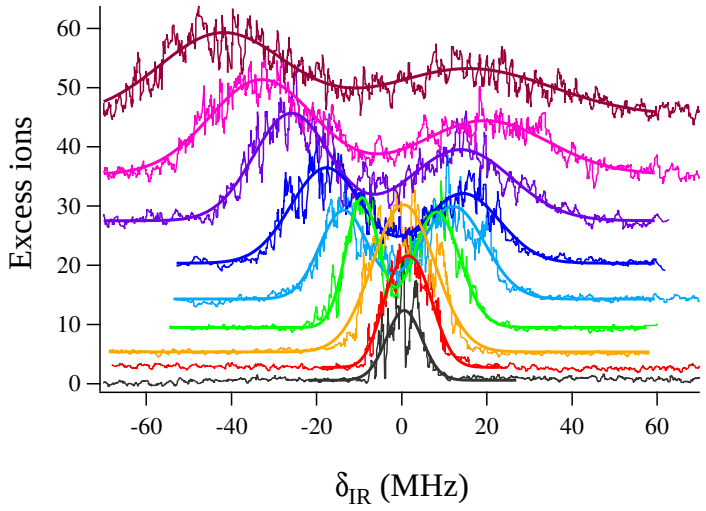

Fig. 6. Spectra versus the IR detuning, and fit by two Lorentzian lineshapes, of the ions produced by the $6^2P_{3/2} \rightarrow 52^2S_{1/2}$ IR excitation, with an offset on the vertical scale. A constant ion number is produced by the blue laser photoionization, and the excess number produced by the IR radiation is plotted. The ion absolute number is determined with a fifteen percent accuracy. Parameters: $\Omega_{IR} = 0.04$ MHz; blue laser driving the $5^2S_{1/2} \rightarrow 6^2SP_{3/2}$ transition at $\delta_{bl} = 0$ MHz, of the blue laser driving, and Ω_{bl} Rabi frequency increasing from the bottom to the top between 10 and 80 MHz in 10 MHz steps; laser pulse length 10 μs. The transition centered at $\delta_{IR} = 0$ at low Ω_{bl} values, increasing Ω_{bl} splits into the two Autler-Townes components.

4.4. Ion created electric field

The Rydberg excitation spectra are modified by the presence of ions created by 6^2P photoionization and by black-body radiation ionization of Rydberg states, the Penning ionization rate being negligible for our experimental conditions. We have observed these modifications while probing the Autler-Townes splitting of the $6^2P_{3/2}$ state with an IR transition to the Rydberg state.

The observation of Autler-Townes splitting allows a direct measurement of the Rabi frequency for a two-state system, as applied in Refs. [18, 19], and the Rabi frequency precise knowledge is necessary for an efficient Rydberg excitation. Example of the Autler-Townes split spectra are shown in Fig. 6 for the two-photon $5^2S_{1/2} \rightarrow 6^2P_{3/2} \rightarrow 52^2S_{1/2}$ transition while scanning the IR laser frequency at constant δ_{bl} and Ω_{bl} values. As expected, the Autler-Townes splitting of the IR absorption line into two components at large values of Ω_{bl} was observed, in agreement with the Autler-Townes prediction.

In Fig. 7 the measured positions of Autler-Townes peaks are plotted versus the blue laser power/Rabi frequency at $\delta_{bl} = 0$ and $\delta_{bl} = -10$ MHz, in (a) and (b) respectively. The dashed lines in the figures are the theoretical predictions from the Eq. (7) by deriving the blue laser Rabi frequency from the laser power and beam waist. The measured peak positions show a systematic shift towards the red. Also plotted are the measured middle frequency of the Autler-Townes peaks. While the Autler-Townes theory predicts a constant position at fixed blue detuning, a systematic shift of the middle frequency towards the red was measured.

This shift originates from the Stark shift of the $52^2S_{1/2}$ Rydberg state associated to the ion

#137237 - $15.00 USD Received 1 Nov 2010; revised 24 Nov 2010; accepted 2 Dec 2010; published 17 Mar 2011

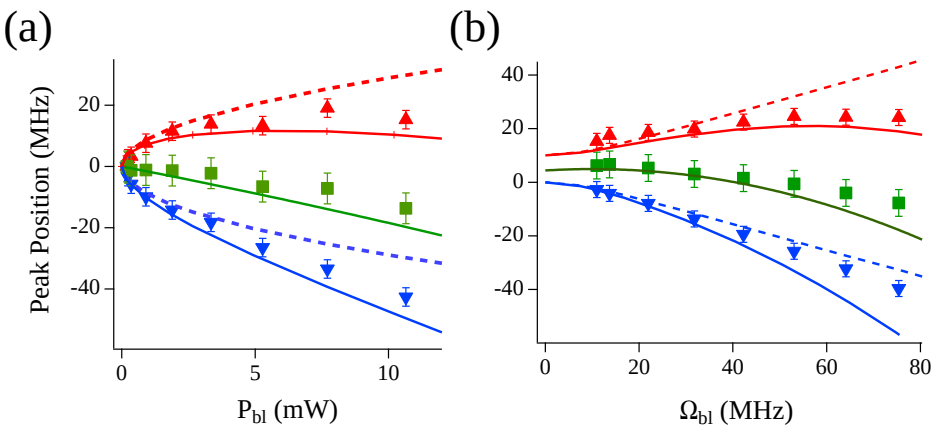

Fig. 7. Measured shifts of the $52^2S_{1/2}$ Autler-Townes peaks (red upside and blue downside triangles) and of the spectrum middle point (green squares) in (a) versus the blue laser power at $\delta_{bl} = 0$, and in (b) at $\delta_{bl} = -10$ MHz versus the blue Rabi frequency. The dashed lines report the predicted Autler-Townes shifts as a function of the blue laser power in the absence of an ion created electric field. The continuous green central line reports the prediction for the $52^2S_{1/2}$ Rydberg state Stark shift produced by the ion created electric field, see text. The continuous lines report the predicted Autler-Townes shifts as a function of the blue laser power including the shift of IR transition produced by the ion created electric field.

created electric field. As the ions are originated mainly from the absorption of one blue photon from the intermediate $6^2P_{3/2}$ state, their number increases with the blue laser power leading to an increasing Stark shift. For instance at $\Omega_{bl} = 60$ MHz, two hundred ions are created by the blue laser photoionization and they produce a measured offset on our signals. We estimated the Stark shift produced by the ions (i) supposing all the ions remain within the cold atom cloud; (ii) determining an average electric field acting on the Rydbergs atoms for the case of ions uniformly distributed within the cloud volume. We verified that the electric repulsion between two ions is not large enough to expel them from the cloud within the excitation laser pulse. The Stark shift predicted by this simple model is represented by the central continuous line in Figs. 7a and 7b with a very good agreement with the measured shift, given the approximations included into our model. In addition the ions are not exactly distributed uniformly within the cloud and their spatial distribution follows the Gaussian profile of the blue laser. By calculating the sum of the Stark shift and of the Autler-Townes shifts we obtain the continuous lines of the Figures in good agreement with measured values. The observed broadening of the Autler-Townes peaks is in agreement with an inhomogeneous distribution of the electric field due to the ions.

The Autler-Townes spectra of Fig. 6 show an asymmetry in the peak heights. Equation (9) shows that for $\delta_{bl} = 0$ the two peaks should have the same height, and instead the red shifted one is more intense. This asymmetry was observed also for the spectra recorded at $\delta_{bl} \neq 0$. We don't have a clear explanation of the asymmetry. In the antiblockade experiments and theory by [30] and [21], respectively, this asymmetry is evidence of antiblockade. However owing to the dipole interaction in n^2S states, in our case the antiblockade should lead to a larger height for the blue shifted peak. An asymmetry in the heights of the Autler-Townes peaks was also observed in [19] and interpreted as an imperfect control of the excitation laser detuning from

#137237 - $15.00 USD Received 1 Nov 2010; revised 24 Nov 2010; accepted 2 Dec 2010; published 17 Mar 2011

resonance. Our control on the frequency of the excitation laser excludes such an occurrence. The role of the ion created electric field requires a careful analysis, and it may be postulated that the electric field modifies the Rydberg-Rydberg interactions and influences the antiblockade.

5. Conclusion

We have investigated Rydberg spectra of ultracold rubidium atoms in a MOT, in order to probe the electric field control present in a set-up based on a quartz cell. This apparatus has the large optical access which is required for Bose-Einstein condensation and the application of a three-dimensional optical lattice. The voltage applied to plates external to the cell in order to ionize the Rydberg states and to collect the ions, creates electric charges on the cell walls. Those charges remained on the walls with a typical ten minute lifetime. We avoided the creation of those charges by applying the voltage as a few microsecond pulse. Using this approach we performed investigations of excitation spectra to Rydberg states with $n = 30-85$ at various electric fields and demonstrated a control of the field at the few mV cm^{-1} level. This flexible control of the electric field matches the requirements of Rydberg excitation for quantum information applications.

The radiation used to excited the rubidium atoms from the ^{2}S state to the 6^2P state also causes the photoionization of atoms in the 6P state. These ions generated an internal electric field which modifies the excitation spectra. Clear evidence of this internal electric field was obtained by studying the Autler-Townes spectra on the Rydberg excitation at increasing values of the blue laser light. This ion production causes a deformation of the Rydberg spectra and is unwanted for quantum information applications. For such a target, the ion production is drastically reduced by detuning the blue laser out of resonance with $5^2\mathrm{S}\rightarrow 6^2\mathrm{P}$ transition, as experimentally verified. For a blue detuning of 1 GHz, the available blue/IR laser intensities lead to a 0.1 MHz two-photon Rabi frequency, large enough for efficient Rydberg excitation.

The extension of Rydberg excitation presented here to ultracold atoms spatially localized inside an optical lattice will be the topic of our future investigation.

Acknowledgements

We gratefully acknowledge funding by the EU STREP project ”NAMEQUAM”, the EMALI European Network, a CNISM “Progetto Innesco 2007” and a MIUR PRIN-2007. The authors thank A. Chotia for help in a preliminary investigation.

#137237 - $15.00 USD Received 1 Nov 2010; revised 24 Nov 2010; accepted 2 Dec 2010; published 17 Mar 2011